Sea ice strength development from freezing to melting in the Antarctic marginal ice zone

F. Paul*, T. Mielke†, R. Audh# and D. C. Lupascu†

* Institute for Materials Science and Center for Nanointegration Duisburg-Essen (CENIDE)
University of Duisburg-Essen
Essen, Germany
e-mail: felix.paul@uni-due.de

Marine Research Institute
University of Cape Town
Cape Town, South Africa
e-mail: ADHRIE001@myuct.ac.za

† Institute for Materials Science and Center for Nanointegration Duisburg-Essen (CENIDE)
University of Duisburg-Essen
Essen, Germany
e-mail: doru.lupascu@uni-due.de, tommy.mielke@uni-due.de

Key words: Sea ice strength, compressive strength, Antarctic marginal ice zone

Abstract: *Sea ice growth in the Marginal Ice Zone of the Antarctic is one of the largest annual changes on earth with a huge impact on the global climate and ecology system [1]. The principles of sea ice growth and melting in the MIZ of the Antarctic are not yet as well researched as their polar counterparts in the north [2]. For this study, pancake ice, consolidated ice and floe ice were analyzed with a compression test in July, October and November 2019 in the marginal ice zone of the Antarctic. Newly formed pancake ice in July showed the highest compressive strength in the bottom layer (3 MPa), whereas consolidated ice was strongest at the top (5 MPa). Consolidated ice in October and November had the highest compressive strength in a middle layer with up to 13.5 MPa, the maximum strength at the top was 3 MPa. Floe ice, consisting of destroyed pack ice, did not show a clear strength development over sea ice depth.*

1 INTRODUCTION

Sea ice growth in the Marginal Ice Zone of the Antarctic is one of the largest annual changes on earth with a huge impact on the global climate and ecology system [1]. The principles of sea ice growth and melting in the MIZ of the Antarctic are not yet well researched. The annual freezing-thawing cycle can be divided into two parts. The first part is the pancake ice cycle, which describes the sea ice growth process in four steps [3]. The melting process is the second part and is dominated by the ice-ocean albedo feedback [4]. Both processes combined, as shown in Figure 1, can explain the full annual growth and melt process in the MIZ of the Antarctic.

https://doi.org/10.4995/YIC2021.2021.12249

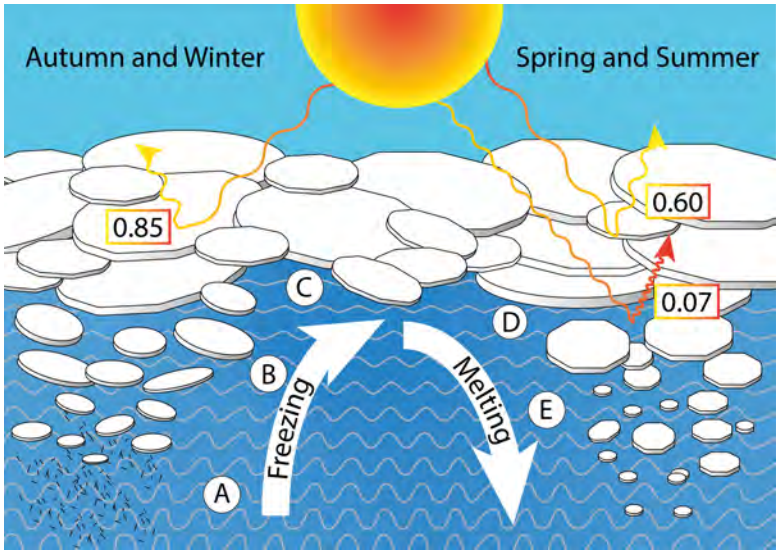

Figure 1: Full-year pancake cycle in the MIZ of the Antarctic. A) Freezing starts with the formation of frazil ice, which develops into grease ice. B) Grease ice grows thicker and starts to form ice floes named pancake ice due to their round appearance. Waves lead to pancake rafting and get attenuated by the ice cover. C) Closed ice cover overcast by snow with an albedo of 0.85. D) The ocean is still completely covered by ice. Solar radiation leads to the melting of the ice cover from the top (Albedo decreases to 0.60) and from the bottom. The bottom starts melting due to the ice-ocean albedo effect. E) Waves break up the ice and release ice floes.

Two prerequisites must be fulfilled for the beginning of sea ice growth: The water must be supercooled *and* under turbulent conditions. If both prerequisites are met, the growth of frazil ice takes place. Frazil ice, which appears as grease ice, a grey milky layer at the surface, is the first step in the annual freezing process. If a sufficient number of frazil ice crystals has formed, the crystals stick together and form flocs of ice. Flocs of frazil ice develop into larger agglomerations of crystals, forming first pans of ice. The size of pancakes varies between a few centimeters for the first pans up to 5 m in diameter for fully grown so called pancakes [5]. Pancakes get rafted by ocean waves and wind, starting to form larger ice floes by pancakes freezing together. The bonding process between the pancakes has not been observed in the laboratory or field yet and is therefore referred to as a welding mechanism [6]. A growing sea ice layer at the ocean surface attenuates the ocean waves, leading to a calmer ocean [7]. When the ocean waves are sufficiently damped, the ice cover freezes up completely. Snow at the sea ice surface increases the albedo of the ice cover to 0.85, preventing the ice and the ocean from absorbing energy from solar radiation. In contrast to snow covered ice, seawater has an albedo of only 0.07. As solar radiation gets stronger, the ocean absorbs most of the solar energy, which increases the water temperature. An increasing water temperature melts the ice from the bottom side, while the melting snow at the top decreases the albedo to 0.60 and lower [8]. As the ice gets weaker due to the melting from the bottom side, the ice breaks up and floes form, which then drift freely in the ocean.

This study will focus on the strength development of sea ice in the full-year pancake cycle, which has an effect on the formation, durability and break-up process of sea ice. This study presents the whole year cycle of freezing and thawing in 2019, enabling a direct comparison between the steps in the full-year pancake cycle.

Up to now, only a few tests have been conducted on sea ice in the Antarctic region. The maximum uniaxial compressive strength reported was 4.5 MPa in the melt season and the mean compressive strength was 2.35 MPa. In this case, the compressive strength was tested

immediately after sampling and showed the strongest layer in the center part of the ice floe [9]. Ice collected by Urabe and Inoue showed the same behavior, even though the samples were tested after long time storage in a cold room. The strongest layer was again in the center part of the floe with a maximum uniaxial compressive strength of about 2.5 MPa [10]. Only a few tests were conducted by Vaudrey with a maximum reported value of 9 MPa [11].

This is the first time, that the uniaxial compressive strength is determined in July, October and November of the same year with the same in situ testing equipment.

2 METHODS

The data provided in this study were collected during the SCALE Winter Cruise and SCALE Spring Cruise in 2019. Locations and ice concentrations for the different stations are displayed in Figure 9. The uniaxial compressive strength was determined with a hand stroke uniaxial compression test (GCTS PLT-2W Point Load Testing Device, GCTS Testing Systems, USA). Cores with a diameter of 9 cm and varying lengths were collected. These cores got cut into several cylindrical samples with a height of 13.5 cm. Even though the perfect relation of diameter to height is 1:2.5 it was decided to not reduce the diameter of the samples to avoid changes in the ice structure and proceed with the test as fast as possible after collection. This study kept the same strain rate for all samples in the ductile-to-brittle transition zone (10^{-3} 1/s) to focus on the sea ice strength development over depth.

3 RESULTS

The results are separated into the five stages of the full-year annual pancake cycle. Frazil ice is tested regarding its rheological properties, pancake ice, consolidated ice, and ice floes are tested using the uniaxial compression test device.

3.1 Frazil ice

Grease ice, which consists of lose frazil crystals and small flocs, is the first ice that forms in the freezing process in the MIZ of Antarctica. Frazil ice crystals grow under turbulent and supercooled conditions. The viscosity of grease ice was determined with a rheometer and showed a shear thinning behavior. A higher frazil ice concentration leads to a higher viscosity, which also indicates, that the ocean gets damped by a thicker frazil ice cover. Due to the completely different experimental approach the results for this set of experiments will be published elsewhere.

3.2 Pancake ice

Pancake ice develops from frazil ice. Pancake ice tested in July 2019 had a medium thickness of 0.36 m. The compressive strength increased from top to bottom, this is displayed in Figure 2. The minimum compressive strength for the pancake ice was 1.5 MPa and the maximum compressive strength was 3.1 MPa.

3.3 Pack ice (freezing period)

Three pack ice cores were cut into eight samples and tested in July 2019. The compressive strength was higher for the consolidated ice than for the pancake ice and showed a different profile over the depth (Figure 2). A relatively high compressive strength could be spotted close to the top, followed by a region with a lower compressive strength. The results for pancake ice and pack ice in the freezing period will be published elsewhere.

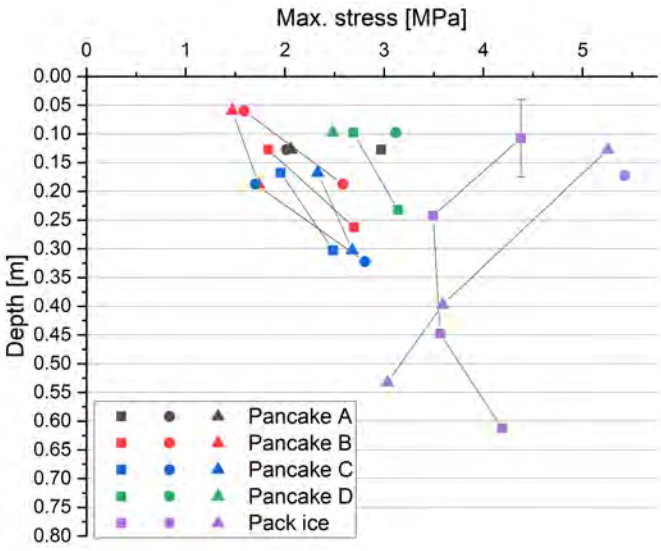

Figure 2: Sea ice strength in July 2019. Symbols connected with a line represent one core. The error bar indicates the length of a sample and is valid for all samples. Further results will be published elsewhere.

3.4 Pack ice (spring)

In total 44 pack ice samples were collected and tested at four different days for the compressive strength during the SCALE spring cruise 2019. The peak load for every sample from the pack ice stations MIZ2, MIZ3, MIZ6 and MIZ7 are displayed in Figure 3. MIZ2, MIZ6 and MIZ7 show an increase of the compressive strength over depth. MIZ3 shows a high compressive strength in a middle layer with a drop in strength beneath.

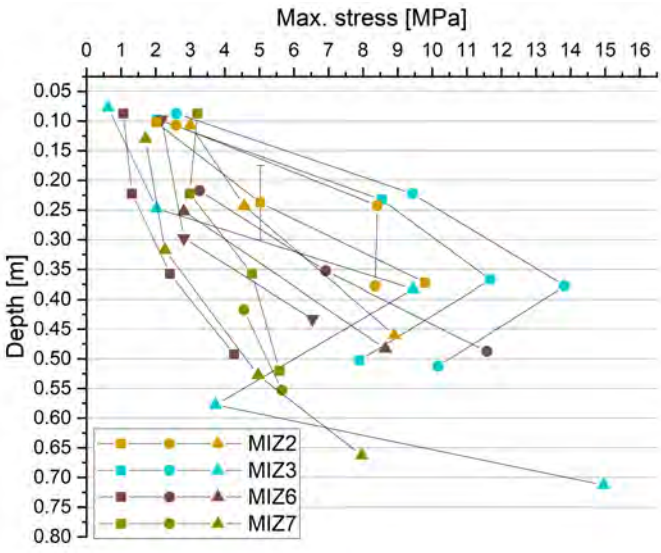

Figure 3: Maximum compressive load in October 2019 for MIZ2 (24.10.2019), MIZ3 (25.10.2019), MIZ6 (29.10.2019) and MIZ7 (30.10.2019). Symbols connected with a line represent one core. The failure occurs somewhere within the sample length of 13.5 cm without knowing the exact location. Therefor the error bar indicates the length of a sample and is valid for all samples shown in the figure.

The temperature gradient over the ice depth is shown in Figure 5. MIZ2 and MIZ3 have a slightly lower temperature at the top than MIZ6 and MIZ7. The bottom temperature is the

same for all stations. Salinity is displayed in Figure 5, showing that the highest salinity is at the top and decreases to a depth of about 30 cm. Below 30 cm all salinity profiles show scattering in the data points with no clear trend. The images of the samples after testing displayed in Figure 4 are typical for the sea ice collected at the stations MIZ2, MIZ3, and MIZ6.

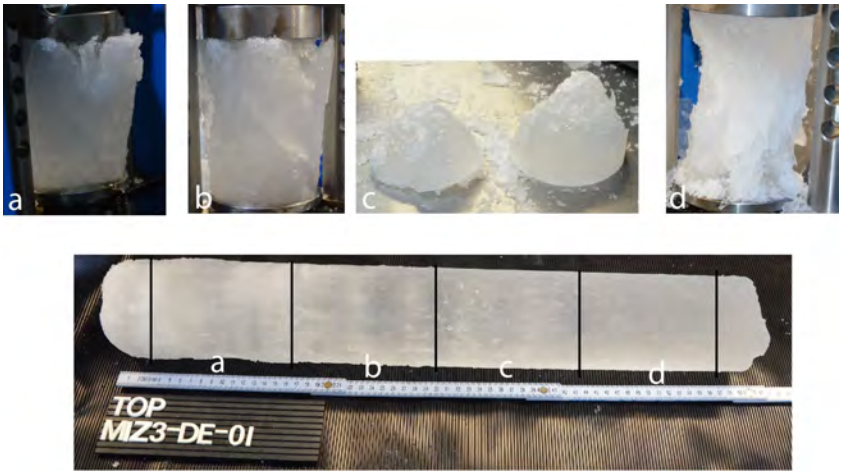

Figure 4: Bottom image of a core from station MIZ3 before preparing the samples. Top images: samples after the compression tests.

Different types of failure were obtained at stations MIZ2, MIZ3 and MIZ6. Sample MIZ3-DE-01-c (Figure 4) as well as sample MIZ3-DE-01-d (Figure 4) show a shear faulting failure. Whereas samples MIZ3-DE-01-a and MIZ3-DE-01-b (Figure 4) did not show terminal failure.

Shear faulting behavior results from confinement across the column [12]. Confinement is induced into the sample by a) the l/d ratio of 1.5, which is lower than the optimal l/d ratio, and b) the rough compression plates, preventing the sample to release stress laterally. The failure mechanism for shear faulting behavior is described in literature as follows: First parent cracks with an angle of 45° to the loading direction are induced into the sample, developing into wing cracks under increasing load. The growth of these cracks is trans-granular and followed by comb cracks. Comb cracks are unique for confined compression tests. They have one fixed end and a free end. If comb cracks are loaded by frictional drag across their free ends they fail. By this failure the load is shed further and starts a chain direction [13, 14]. Wing and comb cracks lead to a measured crack angle of 45° to 65° for all samples which showed a shear faulting behavior in the experiments presented in this study. The samples, which showed a shear faulting behavior during the compressive test, also exhibit the highest compressive strength. Cracks at an angle of 45° to the axis of maximum loading are also visible in the samples MIZ3-DE-01-a and MIZ3-DE-01-b (Figure 4), even though they did not show brittle final destruction of the sample. The samples did not fall apart even after the test, which suggests that the samples show a partwise brittle and ductile behavior. The appearance of 45° cracks to the direction of maximum loading, shows that the ice did not fail in a pure ductile way. Whereas the missing comb cracks, which would lead to an ultimate failure, suggests that the structure within the grain boundaries is not strong enough to allow secondary comb cracks to grow. This might be due to strain relaxation through creep, so that the stress cannot exceed the yield stress [11].

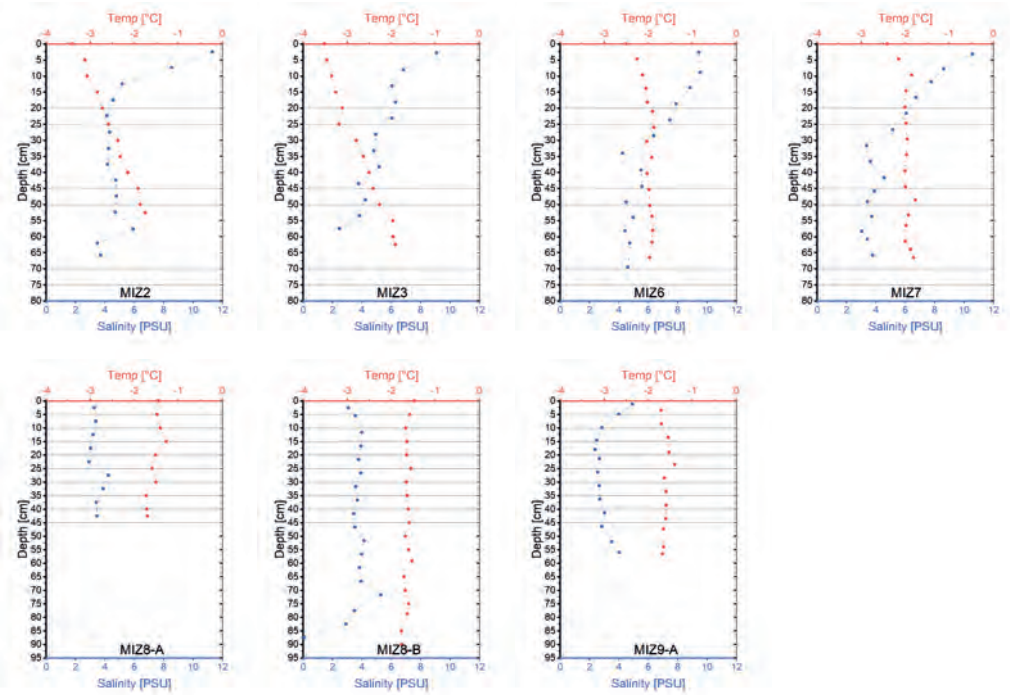

Figure 5: Temperature and salinity profiles for all stations. The first row shows the profiles for the pack ice stations, the second row the profiles of the floe stations. Salinity and temperature measurements were provided by Riesna Audh.

3.5 Ice floes

To reveal more information about the broken ice, eight cores from three different ice floes were tested. The maximum compressive strength is displayed in Figure 6 and shows that the compressive strength is only slightly increasing over depth. The temperature is constant over the ice core length and the salinity varies in a narrow range between 3 and 5 PSU.

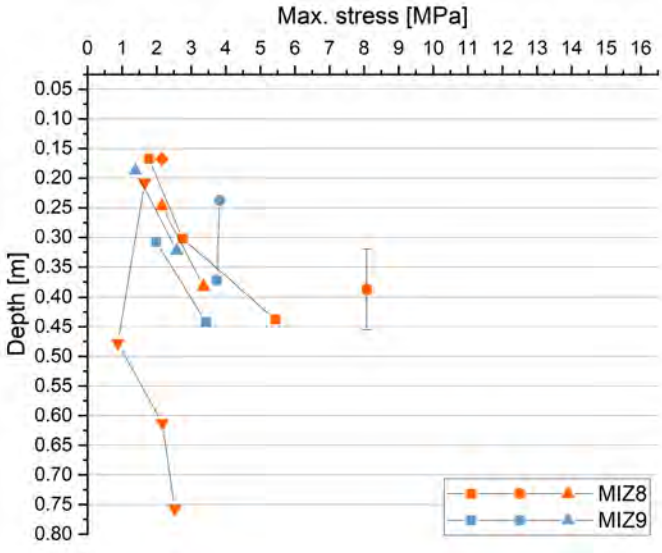

Figure 6: Maximum compressive load for ice floes in November 2019 at MIZ8 (01.11.2019) and MIZ9 (03.11.2019). Symbols connected with a line represent one core. The failure occurs somewhere within the sample length of 13.5 cm without knowing the exact location. Therefor the error bar indicates the length of a sample and is valid for all samples shown in the figure.

Figure 7 shows, at the bottom, an image of an uncut core from an ice floe and, at the top, images after the compression test had been conducted. Figure 7 was chosen, because it is representative for all floe stations from the spring cruise. It can be seen that the entire core is perforated with holes. The holes are distributed over the whole core length, they are visible at the top and bottom of the core. From the holes it can be concluded, that melting takes place from the bottom due to the warmer ocean as well as from the top, due to solar radiation. The top left-hand side sample (Figure 7 a)) deforms comparable to the top samples from Figure 4, whereas the bottom sample shows a different behavior than samples from previous stations. It looks like the top right hand side sample splits into several pieces of ice, along the brine channels. Suggesting, that the weakest bonding during the melting period is between the brine channels.

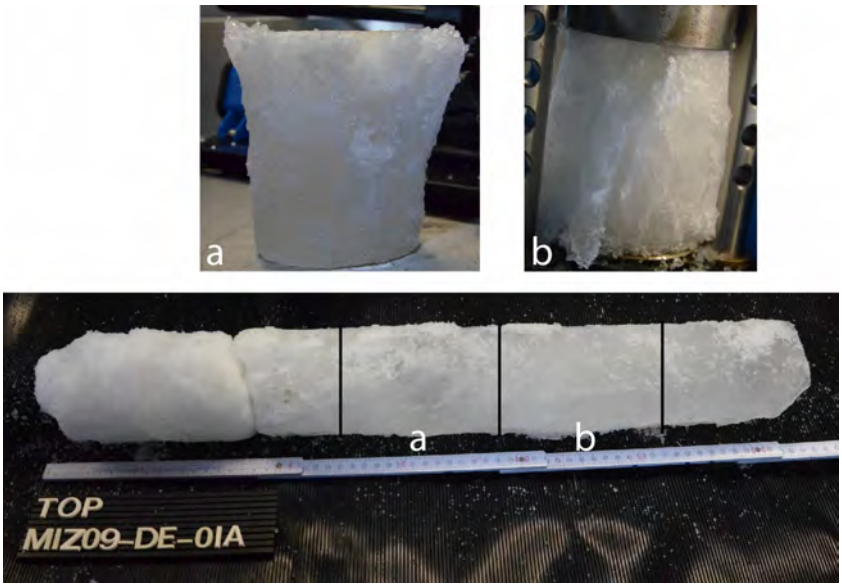

Figure 7: Bottom image of a core from station MIZ9 before preparing the samples. Top image: Samples after the compression test.

4 DISCUSSION

The compression strength of pancake ice is characterized by a low compressive strength at the top followed by an increase of strength over depth. The transition from pancake to pack ice is marked by a higher overall compressive strength. Furthermore, the compressive strength for the pack ice during freezing does not increase monotonously over depth but has a peak for the sample taken from the (Figure 2). This change in sea ice strength for the top sample from 3 MPa and lower for pancake ice to over 4 MPa for the pack ice can be explained by a temperature difference of about 6 °C. A temperature difference in this order of magnitude can lead to an increase of compressive strength by about 1.8 MPa [15].

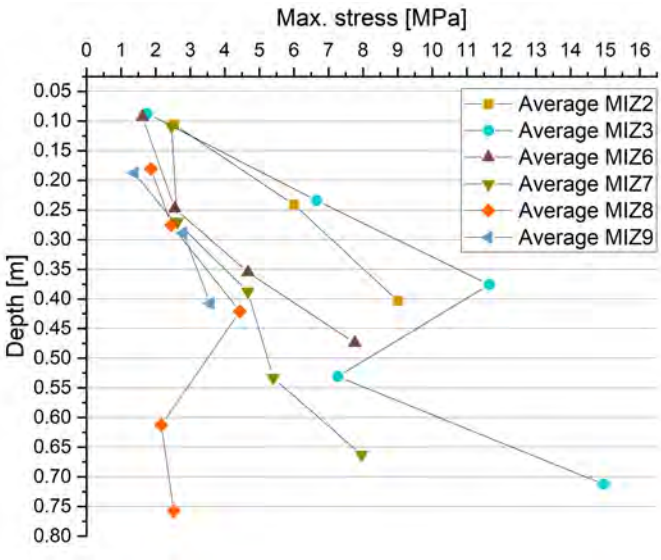

Figure 8: Average compressive strength at each station.

The next step in the full-year pancake cycle is the older pack ice during or shortly before melting. The fact that the ice at MIZ3 has the highest uniaxial compressive strength and the lowest temperature suggests, that it is the least melted station. Station MIZ2 shows a lower compressive strength and a slightly higher temperature compared to MIZ3. At the top samples it is not clear which station has a higher compressive strength in the layers underneath. But the samples in a depth between 20 to 25 cm show a smaller increase in compressive strength for MIZ2 than for MIZ3. The average compressive strength increases for samples from a depth between 10 and 15 cm to samples from a depth between 20 to 25 cm is 3.5 MPa for MIZ2 and 4.9 MPa for MIZ3. Cores collected at MIZ6 and MIZ7 do not show a strong increase from the first to the second sample, but still show an increase for the third sample. Even though the temperature does not differ in a depth of 40 cm and deeper, the compressive strength is further decreasing over depth (Figure 8). The last two ice floe stations MIZ8 and MIZ9 show a similar compressive strength as the ice from MIZ7. MIZ8 differs from MIZ7 by a weaker compressive strength below a depth of 45 cm. The ice floe at MIZ9 was already too short to test below 45 cm but shows the same compressive strength in the top part as MIZ6, MIZ7 and MIZ8. This leads to the assumption, that MIZ6 and MIZ7 are on the verge of breaking apart, a precise time or breaking mechanism cannot be pointed out in this study. It is suggested, that storms or waves will lead to the final ice break up [16, 17].

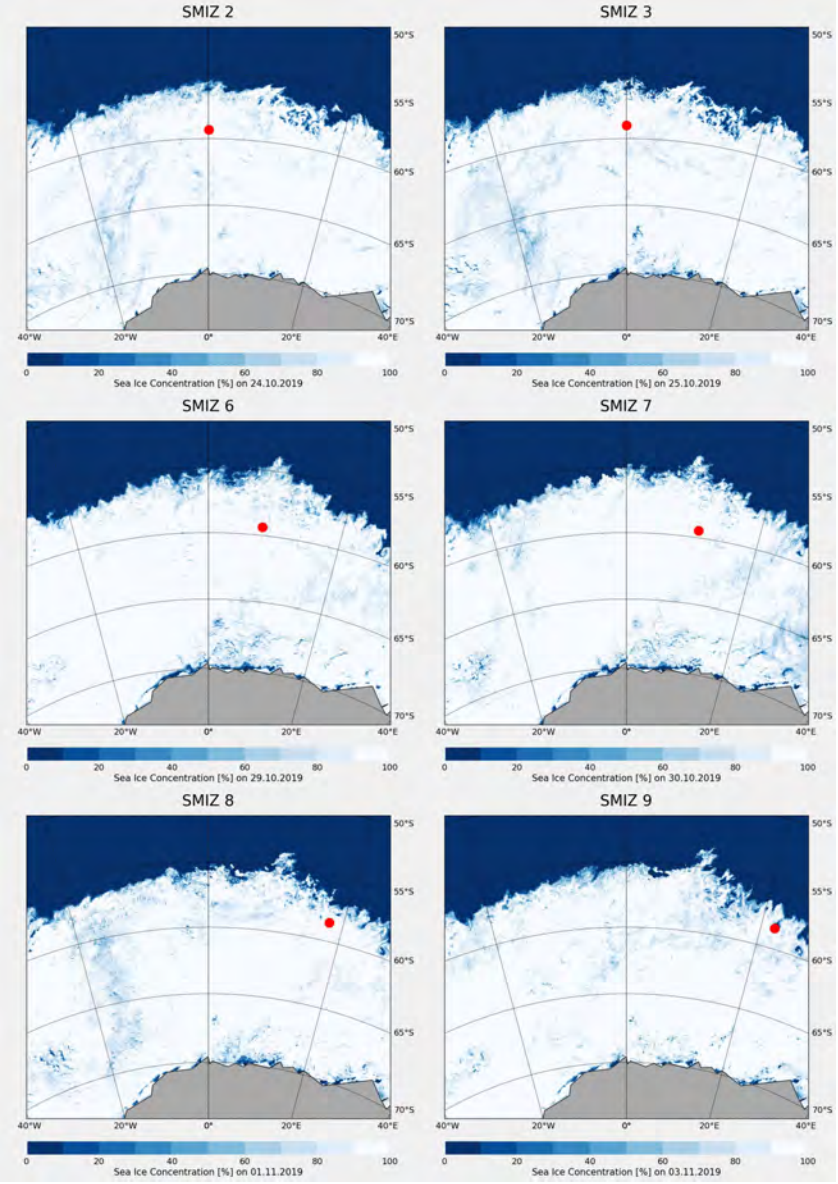

Figure 9: Sea ice concentration at the different stations. The ships position is marked with a red dot.

5 CONCLUSIONS

Data for the compressive strength of sea ice during the freezing and melting cycle of the Marginal Ice Zone of the Antarctic were presented. Samples from pancake ice, pack ice during freezing, pack ice during melting and ice floes were collected.

- The compressive strength of pancake ice increases over the sea ice depth.
- In contrast to the compressive strength in pancake ice, pack ice in the freezing period has a strong compressive strength at the top, followed by a weaker compressive strength underneath.
- Pack ice in the melting period has a comparable compressive strength for the top 15 cm, independent of the melting progress in the sea ice underneath. A maximum in compressive strength was measured in a depth between 35 to 40 cm.

- During the melting process, the compressive strength decreases until it reaches a constant strength over the sea ice depth. If the compressive strength is sufficiently decreased, the pack ice breaks apart and forms ice floes.
- The compressive strength in pack ice, which is estimated to break apart soon, and that of ice floes can be similar.

6 ACKNOWLEDGEMENTS

The SCALE cruises are funded by the South African National Research Foundation (NRF) through the South African National Antarctic Programme (SANAP), with contributions from the Department of Science and Innovation and the Department of Environmental Affairs. We are very grateful to the teams that have contributed to the success of the SCALE cruise in particular under the guidance of Marcello Vichi and Jörg Schröder.

REFERENCES

[1] K. Mezgec, B. Stenni, X. Crosta, V. Masson-Delmotte, C. Baroni, M. Braida, V. Ciardini, E. Colizza, R. Melis, M. C. Salvatore, M. Severi, C. Scarchilli, R. Traversi, R. Udisti, and M. Frezzotti, "Holocene sea ice variability driven by wind and polynya efficiency in the Ross Sea," *Nature Communications*, vol. 8, no. 1, p. 1334, Dec. 2017.

[2] G. W. Timco and W. F. Weeks, "A review of the engineering properties of sea ice," *Cold Regions Science and Technology*, vol. 60, no. 2, pp. 107–129, Feb. 2010.

[3] M. A. Lange, S. F. Ackley, P. Wadhams, G. S. Dieckmann, and H. Eicken, "Development of Sea Ice in the Weddell Sea," *Annals of Glaciology*, vol. 12, pp. 92–96, 1989.

[4] S. Nihashi and D. J. Cavalieri, "Observational evidence of a hemispheric-wide ice–ocean albedo feedback effect on Antarctic sea-ice decay," *Journal of Geophysical Research*, vol. 111, no. C12, p. C12001, Dec. 2006.

[5] M. J. Doble, "Pancake ice formation in the Weddell Sea," *Journal of Geophysical Research*, vol. 108, no. C7, p. 3209, 2003.

[6] L. A. Roach, M. M. Smith, and S. M. Dean, "Quantifying Growth of Pancake Sea Ice Floes Using Images From Drifting Buoys," *Journal of Geophysical Research: Oceans*, vol. 123, no. 4, pp. 2851–2866, Apr. 2018.

[7] B. R. Sutherland and N. J. Balmforth, "Damping of surface waves by floating particles," *Physical Review Fluids*, vol. 4, no. 1, p. 014804, Jan. 2019.

[8] D. K. Perovich and C. Polashenski, "Albedo evolution of seasonal Arctic sea ice: ALEDO EVOLUTION OF SEASONAL SEA ICE," *Geophysical Research Letters*, vol. 39, no. 8, pp. n/a–n/a, Apr. 2012.

[9] S. Kivimaa and P. Kosloff, "Compressive strength and structure of sea ice in the Weddell Sea, Antarctica," *Transactions on the Built Environment*, vol. 5, pp. 331–342, 1994.

[10] N. Urabe and M. Inoue, "Mechanical Properties of Antarctic Sea Ice," *Journal of Offshore Mechanics and Arctic Engineering*, vol. 110, no. 4, pp. 403–408, Nov. 1988.

[11] K. D. Vaudrey, "Ice engineering - Study of related properties of floating sea-ice sheets and summary of elastic and viscoelastic analyses," CIVIL ENGINEERING LABORATORY, Port Huencme, California, Tech. Rep. ADA051184, 1977.

[12] L. M. Wachter, C. E. Renshaw, and E. M. Schulson, "Transition in brittle failure mode in ice under low confinement," *Acta Materialia*, vol. 57, no. 2, pp. 345–355, Jan. 2009.

[13] E. M. Schulson, "Brittle failure of ice," *Engineering Fracture Mechanics*, vol. 68, no. 17-18, pp. 1839–1887, Dec. 2001.

[14] C. E. Renshaw and E. M. Schulson, "Universal behaviour in compressive failure of brittle materials," *Nature*, vol. 412, no. 6850, pp. 897–900, Aug. 2001.

[15] E. M. Schulson and P. Duval, "Structure of ice," in *Creep and Fracture of Ice*. Cambridge University Press, 2009, pp. 5–29.

[16] A. L. Kohout, M. J. M. Williams, S. M. Dean, and M. H. Meylan, "Storm-induced sea-ice breakup and the implications for ice extent," *Nature*, vol. 509, no. 7502, pp. 604–607, May 2014.

[17] J. J. Voermans, J. Rabault, K. Filchuk, I. Ryzhov, P. Heil, A. Marchenko, C. O. Collins III, M. Dabboor, G. Sutherland, and A. V. Babanin, "Experimental evidence for a universal threshold characterizing wave-induced sea ice break-up," *The Cryosphere*, vol. 14, no. 11, pp. 4265–4278, Nov. 2020.